JOURNAL OF PROPULSION AND POWER
Vol. 14, No. 3, May–June 1998

Methodology to Solve Flowfields of Plug Nozzles for Future Launchers

Francesco Nasuti* and Marcello Onofri†
University of Rome "La Sapienza," Rome 00184, Italy

In the development of future launchers, in particular the single stage to orbit launcher, the use of plug nozzles looks promising because of the possibility of improving performance; therefore the capability to achieve accurate evaluations of the relevant flowfields is required. Nevertheless, because of typical flow features, analyses performed by the common computational fluid dynamics methods lead to uncertain and time-consuming results. To circumvent some of these problems an approach based on a simple simulation model that replaces the mixing layer between the nozzle jet and external flow by a contact discontinuity was recently proposed by the authors. Following this approach the complex calculation of the turbulent mixing of flows having different thermodynamic characteristics can be avoided, while correctly accounting for the main features of the flowfield. In this paper this simple model was implemented to compute linear plug nozzle flowfields at different ambient conditions and for different geometries of the plug. The expected flow behavior has been well reproduced and good agreement with the theoretical nozzle performance has been achieved, allowing a performance analysis for some of the main characteristic parameters to be carried out.

Introduction

THE next generation of launch vehicles must provide cheaper access to space. A possible approach relies on the use of a single stage to orbit reusable launch vehicle like the proposed Lockheed Martin Corporation's X-33. The chance of success for these vehicles depends on the development of engines having better performance than those employed so far, as in the case of the possible use of plug nozzles or aerospikes for the X-33 project.[1] The improved performance of these nozzles is of interest for expendable rockets, as shown by the studies on the Ariane 5 evolution, currently being carried out at the European Space Agency (ESA).[2]

The plug nozzles have self-adapting characteristics that can positively circumvent various limits of conventional nozzles. Indeed, to face the decrease of ambient pressure along the mission trajectory, the conventional nozzle design performs on the basis of a compromise between the requirement of a large expansion ratio, to have better performance at high altitudes, and the limitation in the overexpansion at sea level, to avoid uncontrolled flow separation and consequent side loads.

The plug nozzles have been studied since the 1960s and, therefore, advantages, drawbacks, and descriptions of their practical realization are widely addressed in the literature.[2–4] An important drawback is that they are longer and heavier than conventional conical and bell nozzles having the same design pressure ratio. Nevertheless, this drawback can be circumvented by truncating the plug to relatively short lengths, leading only to small losses in total thrust. As a consequence a truncated plug nozzle can still self-adapt to altitude, can be designed for higher expansion ratio than a conventional nozzle without significant weight increase, and may also offer excellent structural integration.

Received June 13, 1997; presented as Paper 97-2941 at the AIAA/ASME/SAE/ASEE 33rd Joint Propulsion Conference, Seattle, WA, July 6–9, 1997; revision received Nov. 6, 1997; accepted for publication Dec. 11, 1997.

*Ph.D., Postdoctoral Fellow, Dipartimento Meccanica e Aeronautica, Via Eudossiana 18. Member AIAA.

†Associate Professor, Dipartimento Meccanica e Aeronautica, Via Eudossiana 18. Senior Member AIAA.

However, the design and analysis of performance of truncated plug nozzles must be better understood because of their complicated flowfield. Their critical regions must be singled out, analyzed, and discussed by both computational fluid dynamics (CFD) and experiments. Unfortunately, it is well known that some critical areas, such as the mixing layer between exhaust jet and external flow and the recirculating flow region behind the base of truncated plugs, are characterized by flow structures such that their full simulation can lead to uncertain and very time-consuming results.

The aim of this study is to show that the plug nozzle flowfields can be computed by simplified and efficient numerical tools. In particular, full-length and truncated linear plug nozzle flowfields are numerically computed by applying a method based on shock fitting and on a simple model of the jet boundary described as a fitted discontinuity. This model was introduced by the authors in the framework of a study on nozzle plumes.[5,6] Because the numerical simulations allow the contributions of different phenomena to separate by integrating the relevant set of equations, analyses of inviscid solutions have been performed first to isolate the main features of the flowfield. Afterward the role of viscosity was analyzed by a comparison between viscous and inviscid solutions.

Geometries and operating conditions of the computed plug nozzles have been proposed by Daimler-Benz Aerospace (DASA) in the framework of the Future European Space Transportation Investigations Programme (FESTIP) promoted by ESA. Experimental tests are currently in progress.

Numerical Method

The simplified simulation model adopted here is based on an original treatment of the turbulent mixing layer between the exhausting flow and the ambient. The model replaces the mixing layer by a contact discontinuity that splits the whole domain into two separated flows. During the numerical transient the discontinuity asymptotically converges toward its steady-state configuration by changing its shape to find a match between the local conditions of the two flows[5] (Fig. 1). This is achieved by enforcing the fact that the pressure and normal components of velocity are continuous across the discontinuity, whereas the tangential component and the entropy are discon-

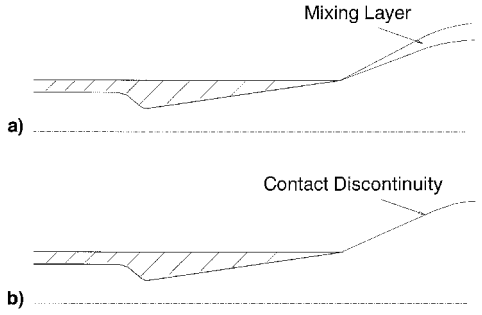

Fig. 1 Sketch of a) physical problem and b) simplified model.

tinuous, allowing the formation of a slip flow along a separation surface between external and internal flows. This method makes it possible to compute the average behavior of the mixing layer and provides useful information when the detailed solution is not mandatory. The numerical method avoids the burden of computational time produced by the mesh clustering in the region of the mixing layer, as well as the necessity of using a chemical nonequilibrium model to correctly simulate the evolution of the two flows when they display very different thermodynamic characteristics. Of course these advantages are not applicable in cases where the growing rate and the mixing characteristic of the shear layer are of interest, for example, as in the case of studies devoted to noise and pollution control. On the contrary, the simplified simulation model is suited to the present study because it is focused on the prediction of the engine performance and, therefore, on the behavior of the main exhaust jet rather than on the thickness and stability of its boundary.

The analysis of plug nozzle flowfields is performed under the assumption of calorically perfect viscous laminar or inviscid gas. The solution is based on the nonconservative form of the Navier–Stokes equations that are integrated by a finite difference, second-order, time- and space-accurate scheme that follows Moretti's $\boldsymbol{\lambda}$ formulation for the convective terms[7] and uses central differencing for the viscous terms.[8] The computation is performed over orthogonal grids patched by means of a multiblock technique. The shocks are treated by a floating shock-fitting technique, recently developed by the authors,[9] based on computations introduced by Moretti.[10]

It should be stressed that the proposed general-purpose model of the mixing layer, whose capability is demonstrated in Ref. 5, can be implemented with codes based on approaches different from the $\boldsymbol{\lambda}$ scheme and particularly with methods based on the conservative form of the governing equations.

Results

The numerical simulations of linear plug nozzles (LPN) concern two reference plug geometries based on different characteristics of the flow exhausting on the plug wall. They have been studied first in their ideal configuration of a full-length plug and then in more practical truncated shapes. Finally, two different plug geometries were computed to investigate some effects of the current plug-design methodologies. For all test cases the working gas is cold air characterized by 1) the ratio of specific heats $\gamma = 1.4$, 2) gas constant $R = 287$ J/K/kg, and 3) chamber temperature $T_c = 320$ K; the ambient gas is quiescent air.

In the case of viscous computations a linear dependence of viscosity μ on temperature is assumed: $\mu/\mu_r = T/T_r$, where $T_r = 288$ K and $\mu_r = 1.786 \times 10^{-5}$ kg/(m·s) are the reference temperature and viscosity, respectively; constant Prandtl number $Pr = 0.72$ is assumed; and the consequent thermal conductivity $k = \mu c_p/Pr$, where c_p is the constant pressure specific heat. Moreover, isothermal wall at $T_w = 300$ K has been assumed.

Full-Length Plug

The analysis of full-length plug nozzles has been performed first to understand ideal plug behavior. These configurations represent reference solutions to evaluate the performance of truncated plug nozzles whose design is based on the same plug geometry.

First Test Case: LPN1

The first test case concerns the computation of the flow over the full-length linear plug nozzle LPN1, which displays a sonic orifice as a primary nozzle exhausting over an ideal contour designed following Angelino's method.[11] The design pressure ratio is PR = 200, obtained as the ratio of chamber pressure $p_c = 8.75$ bar to the ambient pressure $p_a = 0.04375$ bar.

The solution of the inviscid flowfield relevant to the 100% plug length has been computed also for off-design pressure ratios. Figure 2 shows the computed Mach number flowfields that were obtained by decreasing PR from the design value 200 to a value as low as 8.9. The relevant wall pressure behaviors are shown in Fig. 3.

At design conditions (PR = 200, Fig. 2a) the expected flow behavior is obtained: the exhaust jet undergoes a centered expansion at the primary nozzle lip and rotates up to the axial direction. The reflected expansion waves are canceled out by the suitable design of the plug geometry and eventually uniform axial flow is obtained at the plug exit. The corresponding computed wall pressure is a monotonic decreasing function (Fig. 3). The profile of the jet boundary is well computed as a straight line parallel to the x axis, as theoretically expected from the plug design.

At higher ambient pressure the exhaust flow undergoes a weaker centered expansion and turns less than in design conditions. Therefore, the last expansion wave impinges on the plug wall at shorter and shorter distances from the primary nozzle exhaust section (Figs. 2b–2h). Downstream of the last expansion wave, the plug geometry, designed to avoid the reflection of the other expansion waves occurring for PR = 200, generates compression waves. These compression waves interact with the jet boundary, whose consequent turning is shown in Figs. 2c–2h. The result of the interaction of the compression waves with the constant pressure jet boundary is a second centered expansion fan, which makes the flow expand again. In particular, increasing ambient pressure leads to lower expansions at the primary nozzle lip (Figs. 2c and 2d) resulting in more expansion–compression cycles along the plug wall and in smaller amplitudes (Fig. 3).

Because no strong compression waves are produced at the higher PR the calculations do not show any fitted shock.

The self-adaptation process is indicated by the flow at the plug exit section, displaying a nearly axial direction, and an average pressure nearly equal to the ambient pressure. This behavior is also confirmed by the values (Table 1) of the nozzle efficiency η, defined as the ratio of the thrust coefficient C_F to the ideal thrust coefficient $C_{F,i}$. The $C_{F,i}$ is the maximum theoretical C_F achievable at an assigned pressure ratio computed by one-dimensional relations.

The computed efficiency is high in both on- and off-design conditions, and its displacement from 1.0 is of the same numerical accuracy order of the computations for the entire range of explored pressure ratios. As reference values Table 1 shows the efficiency of conventional nozzles designed for the pressure ratio PR_d, computed by one-dimensional relations. These values allows one to quantify the advantages of a self-adaptable nozzle. One of its well-known properties is to show, for the operations at the lower PRs, better efficiency than a conventional nozzle designed for the same PR_d, even without accounting for the well-known problems of a conventional nozzle in highly overexpanded conditions. Another is to show, for the operations at the higher PRs, higher efficiency than a conventional nozzle designed for a lower PR_d.

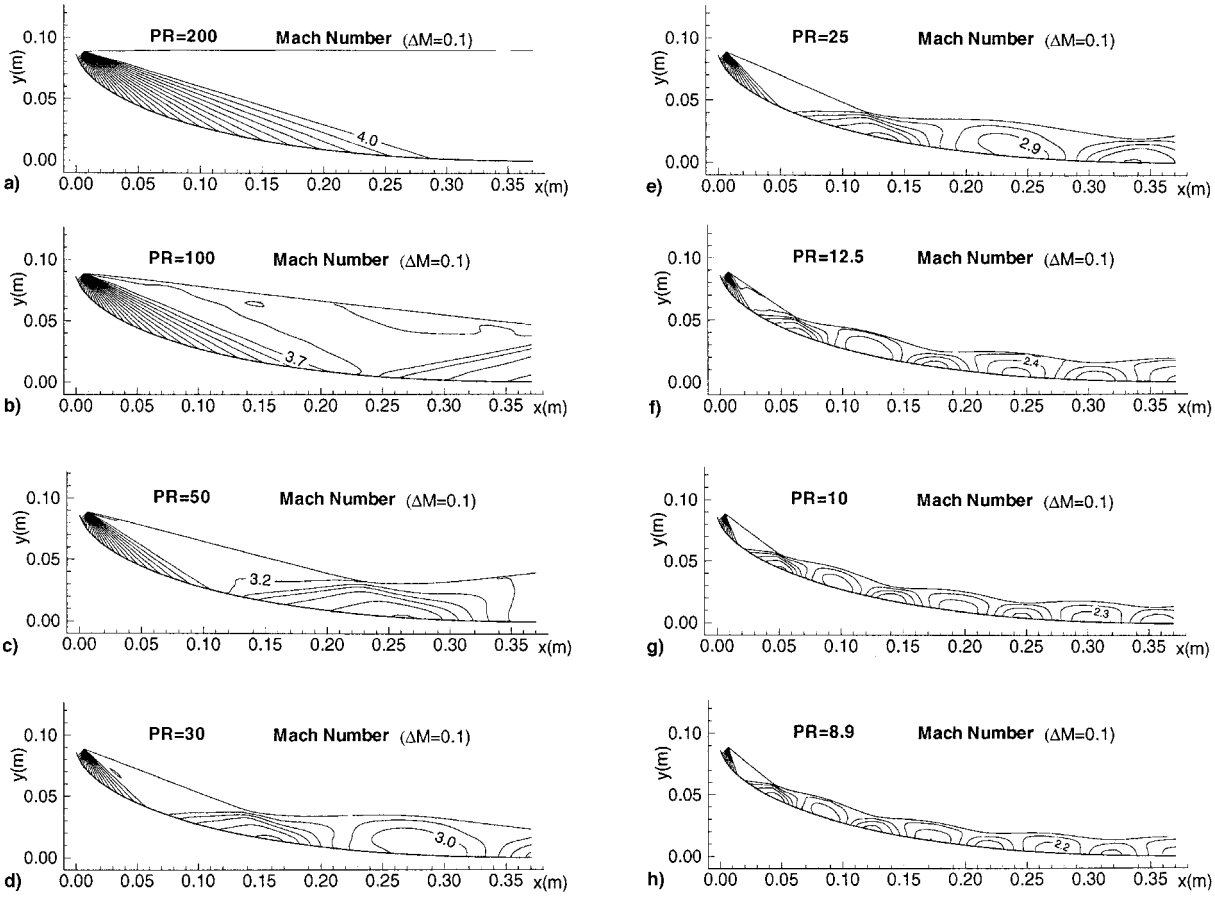

Fig. 2 Full-length LPN1 inviscid computation and Mach number contours for different pressure ratios.

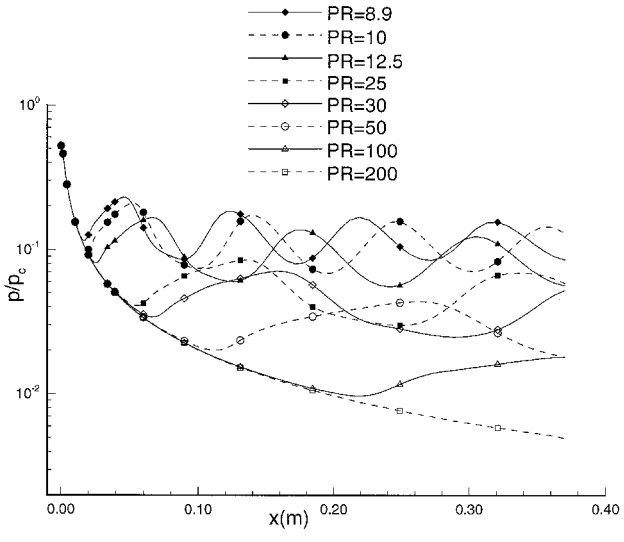

Fig. 3 Full-length LPN1 inviscid computation. Pressure along the plug wall for different pressure ratios.

Second Test Case: LPN2

The second linear plug nozzle (LPN2) considered is characterized by a primary supersonic bell nozzle, expanding at pressure ratio PR = 28.8. In this case the nonuniform flow exhausting from the primary nozzle makes it more difficult to design a plug geometry capable of canceling out all of the impinging waves. The configuration of the plug extension designed by DASA still follows Angelino's approach,[11] but it is smoothly jointed to the primary nozzle contour. As in LPN1 the design pressure ratio is PR = 200, obtained as the ratio of p_c = 8.75 bar to p_a = 0.04375 bar.

Table 1 Efficiency (η) of LPN1 (inviscid computation) and conventional nozzles (inviscid one-dimensional relations)

		PR			
Nozzle	PR_d	8.9	30	200	∞
LPN1	200	0.99	0.98	0.99	0.92
Conventional	200	0.18[a]	0.86[a]	1.00	0.92
Conventional	30	0.92[a]	1.00	0.96	0.86

[a]Conventional nozzle in overexpanded regime.

As shown by Mach number contours in Fig. 4a the flow over the plug features many waves, even in design conditions where a simple wave flow was obtained for the LPN1 case. This depends on several aspects. First, the flow at the exit of the primary nozzle is not uniform, this is because of the symmetric expansion fans coming from the nozzle throat and because of the following compression waves generated by the change of wall curvature downstream of the throat section. Second, these waves interact with the compression waves generated at the exit of the primary nozzle by the concave plug wall curvature. The result of these two phenomena is the formation of stronger compression waves emanating from the plug wall that coalesce in a shock inside the exhaust jet. Finally, farther downstream, this behavior is canceled out by the expansion waves generated at the primary nozzle lip. All of these flow features are more evident if the characteristic net is drawn (Fig. 4b).

The result also shows that the jet boundary does not start horizontal because the pressure value near the primary nozzle wall is higher than the average exit pressure that was considered as a design condition. Afterward, as shown by Fig. 4b, the jet boundary is bent by the expansion waves coming from the lower side of the throat and becomes nearly horizontal until it is reached by the shock wave generated along the plug wall.

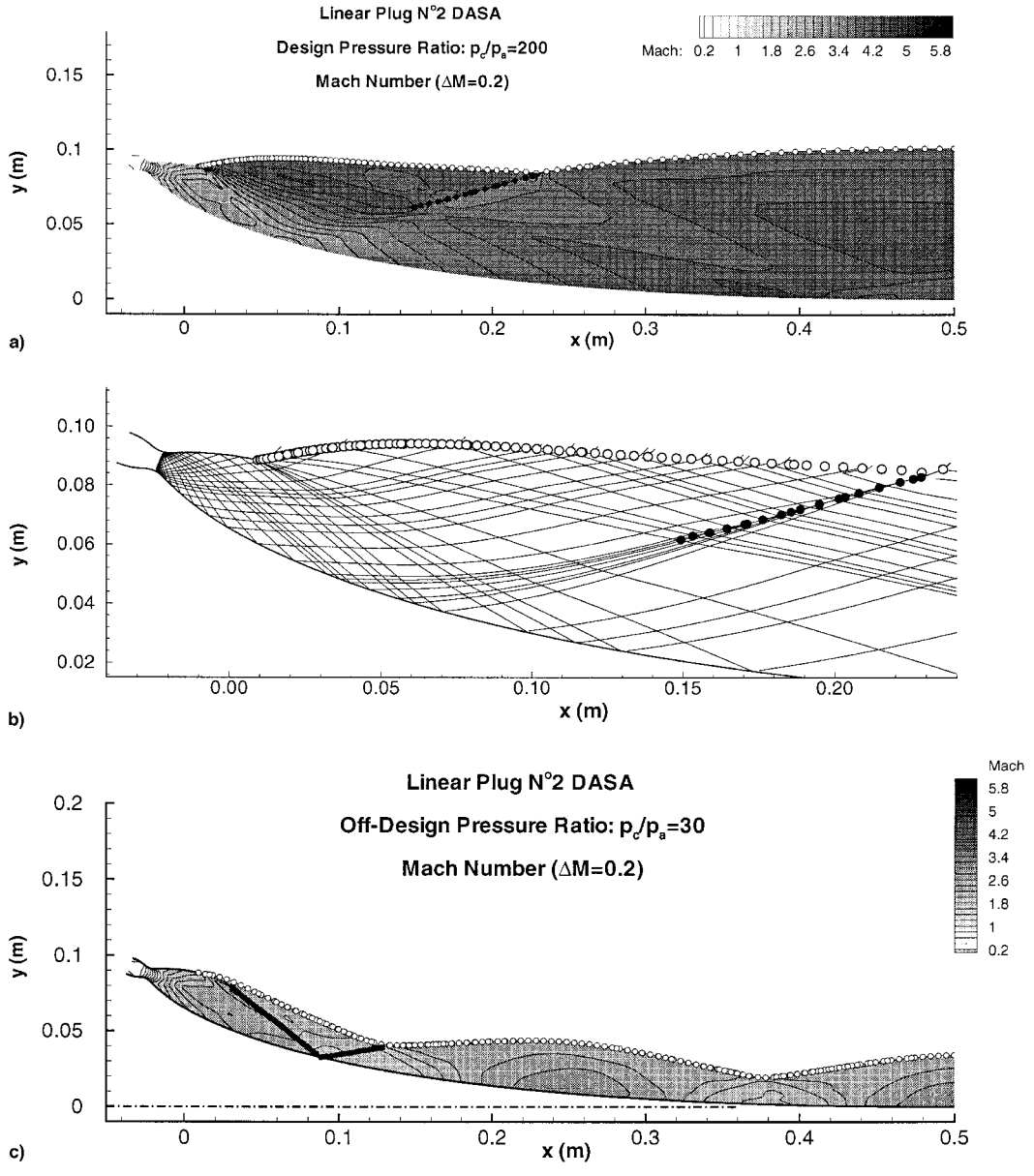

Fig. 4 Full-length LPN2 inviscid computation: a) Mach number contours for PR = 200, b) characteristic net for PR = 200 (enlargement of the primary nozzle lip region), and c) Mach number contours for PR = 30. ●, shocks; ○, jet boundary.

At this point it again turns upward, and at the plug exit the flow is still slightly nonaxial and nonuniform.

Higher ambient pressures lead to narrower jets as shown, for example, for PR = 30 in Fig. 4c. This PR value is close to the minimum pressure ratio to be considered that will allow the primary nozzle to work in underexpanded conditions. The expansion waves coming from the lower side of the primary nozzle throat section are no longer spread by the expansion fan at the primary nozzle lip as in the PR = 200 case. This leads to a smaller curvature radius of the downward turn of the jet just after the nozzle lip. The consequence of this is the generation of compression waves more rapidly coalescing in a shock wave. The generation of this shock wave conceals the phenomena that led to the shock formation in the PR = 200 case. In fact, the combined effect of compression waves from the upper side of the throat region and from the concave wall remains unchanged. However, because the new shock impinges on the plug wall just downstream from the region where that combined effect occurs, the compression waves leaving the plug wall no longer coalesce in a new shock but instead strengthen the reflected shock.

Compared to LPN1, as a result of the higher Mach number at the primary nozzle exit of LPN2 (average M = 2.84), the compression waves find it easier to coalesce in shocks. Nevertheless, in spite of the presence of shock waves in the exhaust jet, there is no major consequence on the nozzle efficiency (Table 2).

Truncated Plug

Truncated plug nozzle flowfields were considered in the second phase of this study. Because of the complex recirculating flow that takes place behind the plug base, doubts can be raised on the quality of the numerical solutions in these regions. Indeed, on one hand, the correct effect of the viscosity is difficult to predict even by viscous simulations because of its dependence on the turbulent model adopted. On the other hand, it is known that inviscid simulations cannot achieve a full-grid convergence when recirculating flows occur independent of the solution method: The exchange of momentum and entropy between main and separated flows is driven by the numerical diffusion at the interface region, which in turn is dependent on the local mesh size used.

A detailed discussion of these and other numerical problems is beyond the scope of this paper, nevertheless a separate study has been carried out and is reported in Ref. 12. Here three aspects are mentioned:

1) The computations have been carried out over orthogonal grids drawn to follow the plug wall turning around its lip (Fig. 5). The number of grid cells has been chosen to predict the dimensions of the bubble of recirculating flow with negligible differences shown by grid refinement.

2) The results are independent of initial conditions as shown by specific tests performed by starting the computations with different flowfields.

3) Because it is known from the numerical studies on base flows[13] that the solution depends on the turbulent model adopted, only viscous laminar flows have been computed here to avoid unclear superimposition of different effects and, therefore, the results have only a qualitative value that is useful to achieve information on the role of the viscous phenomena on nozzle behavior.

The solutions presented here for truncated plug nozzles provide an assessment of the flow structure and nozzle performance and, although the real flowfield may differ in some details, they represent a useful step before progressing to a more intense study using more sophisticated methods.

First Test Case: LPN1

Two different plug lengths have been considered: 10 and 20% of the full length. In the study a larger number of calculations were carried out for the 20%-length case, for which experiments will soon be made available by DASA. To match the experiments the chamber pressure considered is different from the full-length plug case: $p_c = 3.74$ bar.

The results obtained for different ambient pressure values by the inviscid simulation are shown in Figs. 6 and 7. The curves of Fig. 6 show the evolution of the jet boundary shape as the ambient pressure is increased.

Table 2 Efficiency (η) of LPN2 (inviscid computation)

Nozzle	PR_d	PR = 30	PR = 200
LPN2	200	0.98	0.99

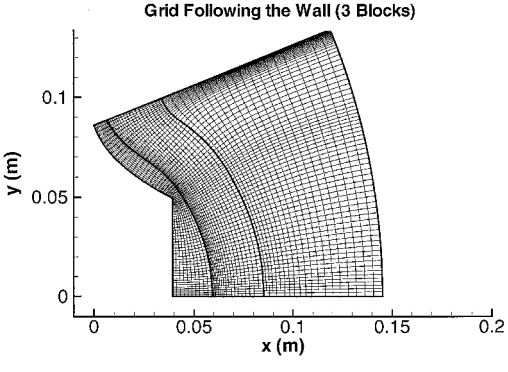

Fig. 5 Orthogonal grids for truncated plug.

The flow structure is characterized by the generation of a second centered expansion at the truncation lip and by an inviscid recirculating zone behind the truncated base of the plug. In the Eulerian model the flow can still turn around the plug corner without detachment. Locally, very high Mach number and low pressure are achieved just downstream of the corner, leading to a strong normal shock followed by flow separation. The preceding mechanism generates the entropy gradient needed to have the Eulerian recirculation bubble that spans behind the base of the plug. Its upper boundary becomes the lower boundary of the main flow that impinges on the symmetry axis at an angle and, therefore, an oblique shock takes place to turn the flow upward. For the lower ambient pressure case (Fig. 7a) this reattachment occurs at $x \sim 0.15$ m and the oblique shock wave propagates downstream, realigning the jet to the axis. The same phenomenon occurs as the pressure ratio decreases (Figs. 7b–7d).

At PR = 100 (Fig. 7b) the main differences are the smaller extension of the first expansion fan (generated at the primary nozzle lip), the consequent smaller region of its interaction with the second expansion fan (generated at the plug lip), and the more uniform flow behind the oblique shock wave. However, the expansion waves coming from the primary nozzle lip still impinge on the recirculation bubble boundary.

When PR = 30 the first expansion fan spans up to the plug lip where the second expansion fan takes place (Fig. 7c). At $x \sim 0.13$ m the second expansion fan interacts with the upper jet boundary, which consequently turns downward. The structure and extension of the recirculation bubble are similar to the PR = 100 case, where there is only a weak effect of the last waves coming from the primary nozzle lip.

The flow structure changes significantly for the lower PRs considered, as shown in Fig. 7d for the case of PR = 8.9. The main feature of the flow is the narrow exhaust jet. In this case the expansion fan that takes place at the primary nozzle lip impinges over a short length of the plug wall. Downstream, successive compressions and expansions take place on the plug surface, following the same behavior already shown for the full-length plug (Fig. 2), with the small-amplitude fluctuations of the wall pressure around the value of the ambient pressure shown in Fig. 3. A similar phenomenon takes place along the lower jet boundary, i.e., the upper boundary of the recirculation bubble. The shock and the following expansion waves coming from the plug lip and from the lower jet boundary hit the upper boundary, are reflected, again hit the lower jet boundary, and so on. The overall effect is the generation of a more open bubble behind the truncation section. In fact, the upper boundary of the bubble starts horizontally and a shock takes place at the plug lip. The shock makes the upper jet boundary turn upward and the boundary reflects the shock as a centered expansion fan. This fan, in turn, is reflected by the lower jet boundary as a shock wave that can be seen in Fig. 7d as the horizontal discontinuity through the main jet at $x \sim 0.12$–0.14 m.

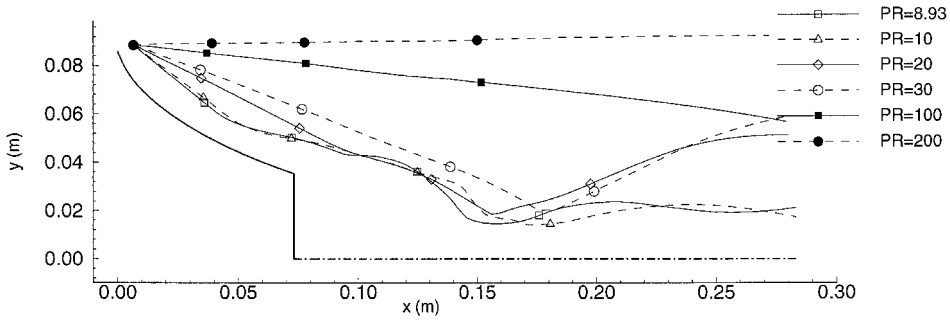

Fig. 6 20%-length LPN1 inviscid computation. Jet boundary for different pressure ratios.

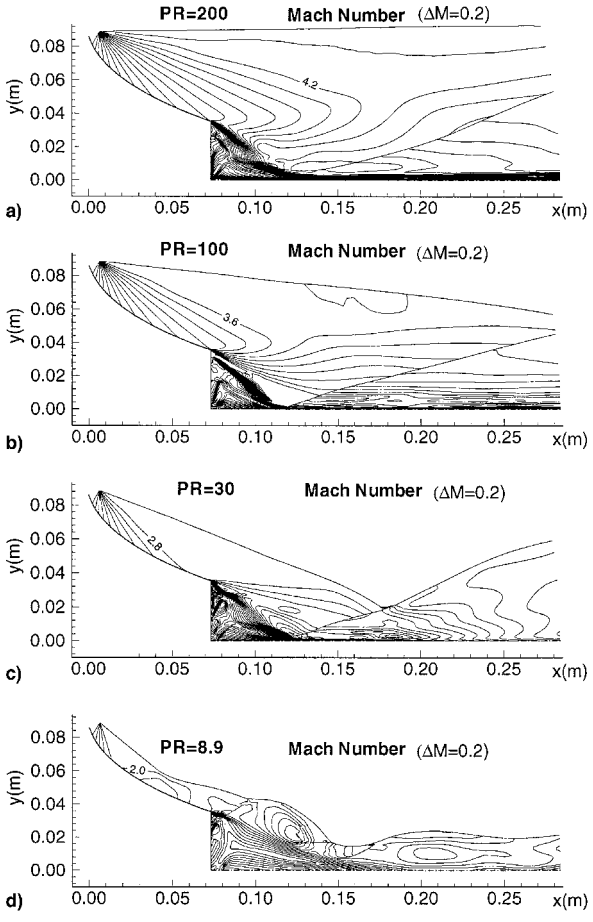

Fig. 7 20%-length LPN1 inviscid computation and Mach number contours for different pressure ratios.

Table 3 Efficiency of full-length and truncated LPN1 (inviscid computation)

	PR				
Length, %	8.9	10	30	100	200
10	——	——	0.75	——	0.95
20	0.89	0.89	0.85	0.94	0.97
100	0.98	0.98	0.98	0.98	0.99

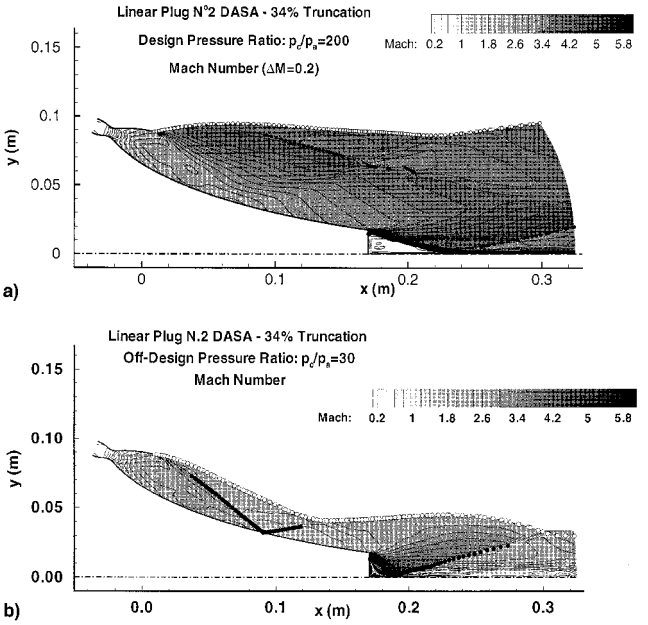

Fig. 8 34%-length LPN2 inviscid computation. Mach number contours, shock points (●), and jet boundary (○) for PR = a) 200 and b) 30.

The efficiency of the preceding nozzle is obviously lower than the full-length one, particularly at the lower PR range (Table 3). Nevertheless, at the higher PRs the values are still of the same order of magnitude as the $PR_d = 30$ conventional nozzle, whose performance can be considered to be representative of a good compromise achievable by fixed geometry conventional nozzles (see Table 1). Because this truncated plug nozzle also works with nearly constant efficiency at low PR, it can still be considered competitive with conventional nozzles as a result of the problems that arise when the latter nozzles work in overexpanded conditions.

On the contrary, for the shortest LPN1 considered (10% length), the nozzle efficiency decreases at such low levels (Table 3) that it can no longer be considered competitive when compared with conventional nozzles.

Second Test Case: LPN2

For the second test case two possible truncations were considered: 34 and 3.5% of the full-length of LPN2. The relevant Mach number contours are shown in Figs. 8 and 9, respectively.

The plug efficiencies shown in Table 4 were computed at the design condition PR = 200 and at an ambient pressure slightly lower than primary nozzle exit pressure (PR = 30). They show that truncation of the plug at 34% of its length does not significantly affect the performance, whereas the shortest plug (truncation at 3.5%) produces a much lower thrust. The reason for the nearly identical performance of 34% and 100% length nozzles is in the small contribution of the base, as a result of its small height. In fact, for PR = 30, the 34%-length LPN2 shows good performance, and its efficiency is only 3–4% lower than the full-length plug.

A different situation is shown in Fig. 9a for the 3.5%-length nozzle. Indeed, there is no plug, but a primary nozzle attached over a base. Such a large base does contribute to the total nozzle thrust, and the effect is a degradation of performance: It is less efficient than a conventional nozzle identical to the LPN2 primary nozzle (compare with the $PR_d = 30$ conventional nozzle in Table 1), also in design conditions, and it is almost 20% less efficient than the ideal nozzle for PR = 30.

Viscous Calculations

In the next phase of the study the role of the viscosity has been considered to analyze the boundary-layer behavior along the plug wall, upstream of the plug lip, and to have a more physical separation mechanism than the inviscid at the plug lip. Moreover, the results provide useful information to assess the capability of the inviscid approach in evaluating nozzle performance.

Figure 10 shows the numerical schlieren for the lower pressure ratio considered (PR = 8.9) in the 20%-length LPN1 case. Along the plug wall, downstream of the region affected by the expansion fan coming from the primary nozzle lip, the compression generated by the concave wall profile makes the flow separate. This is clearly confirmed by the skin friction coefficient (Fig. 11) computed using as reference velocity, density, and viscosity their values in the stagnation (chamber) conditions. Figure 11 indicates that the separation occurs at $x = 15$ mm and reattachment occurs at $x = 40$ mm. Downstream of the separation point a second shock appears, connected with the flow reattachment (Fig. 10). Evidence of flow separation along plug walls also has been discussed in Ref. 14.

The separated boundary layer is shown also by the diagram of Fig. 12, displaying the behavior of wall pressure as a function of the decreasing distance from the symmetry axis for the

Table 4 Efficiency of full-length and truncated LPN2 (inviscid computation)

	PR	
Length, %	30	200
3.5	0.82	0.92
34	0.94	0.99
100	0.98	0.99

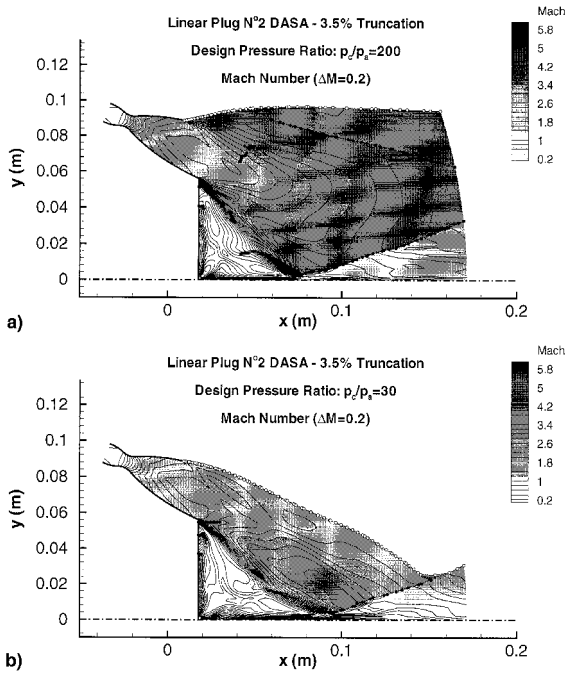

Fig. 9 3.5%-length LPN2 inviscid computation. Mach number contours, shock points (●), and jet boundary (○) for PR = a) 200 and b) 30.

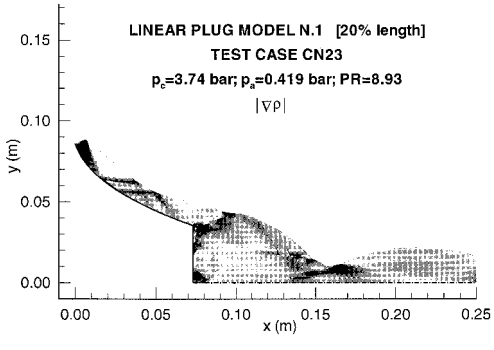

Fig. 10 20%-length LPN1 viscous computation. Numerical schlieren ($|\nabla\rho|$) for PR = 8.9.

viscous and inviscid simulations of the 20%-length LPN1, at PR = 8.9. Figure 12 shows that the viscous and inviscid curves differ at $y \sim 0.06$–0.07 m in the region between flow separation and reattachment. The second difference, at $y \sim 0.05$ m, is caused by the waves coming from the separated region and impinging again on the plug wall after reflection by the jet boundary. Notice that the separated region is very limited and after reattachment the wall pressure behaviors again coincide. This behavior shows that the contribution to thrust of the plug wall is the same in both cases of viscous and inviscid simulation. Another difference is the lack of low-pressure peak in the viscous case. In spite of such a significant difference the average pressure on the base wall ($y < 0.038$ m) is similar. The consequence of this is that the efficiency computed in the viscous laminar case is nearly equal to that computed with the inviscid model (Table 5).

Table 5 Efficiency of truncated plugs (inviscid and viscous computations)

Plug (length)	PR	η (inviscid)	η (viscous)
LPN1 (20%)	8.9	0.89	0.90
LPN2 (34%)	200	0.99	0.99

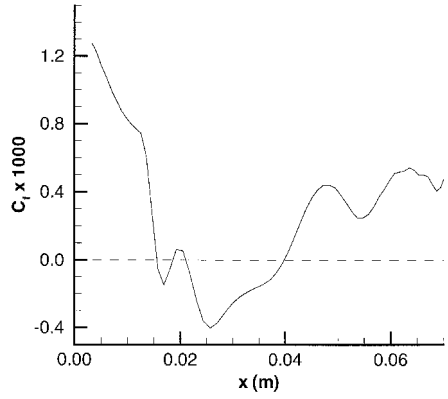

Fig. 11 20%-length LPN1 viscous computation. Skin friction coefficient for PR = 8.9.

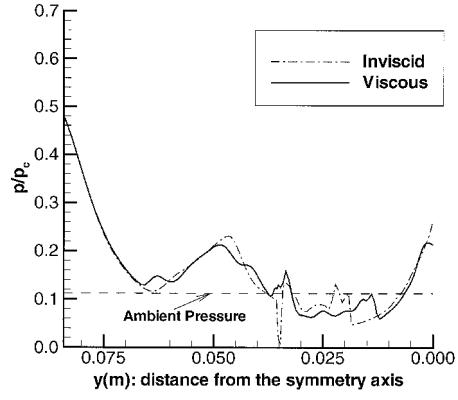

Fig. 12 Wall pressure comparison for viscous and inviscid 20%-length LPN1 computations for PR = 8.9.

The viscous computation of the 34%-length LPN2 leads to analogous results. The comparison of viscous and inviscid solutions is displayed in Fig. 13 by the enlargement of the base region. Figure 13 shows a smaller and more regular wake in the viscous solution that is characterized by a secondary recirculation over the base wall. Such an effect does not yield important variations of the performance in this case because of the small contribution of the base wall, but it could give a significant contribution in the case of a very short plug.

It must be emphasized again that for plug length such that the base height is small compared to the total plug height, the contribution of base pressure is negligible with respect to the overall thrust of the nozzle. This is not the case with short plugs that need an accurate representation of the flow in the base region.

Design Methodologies

Further considerations concern the capabilities of the current methodologies to design the plug nozzle contour. Many available design procedures are based on Angelino's approach,[11] with some specific improvements. They provide geometries of the plug contour by assuming a uniform exhaust jet from the primary nozzle. In this study tests were performed to evaluate the consequences of a nonuniform jet exhausting from the pri-

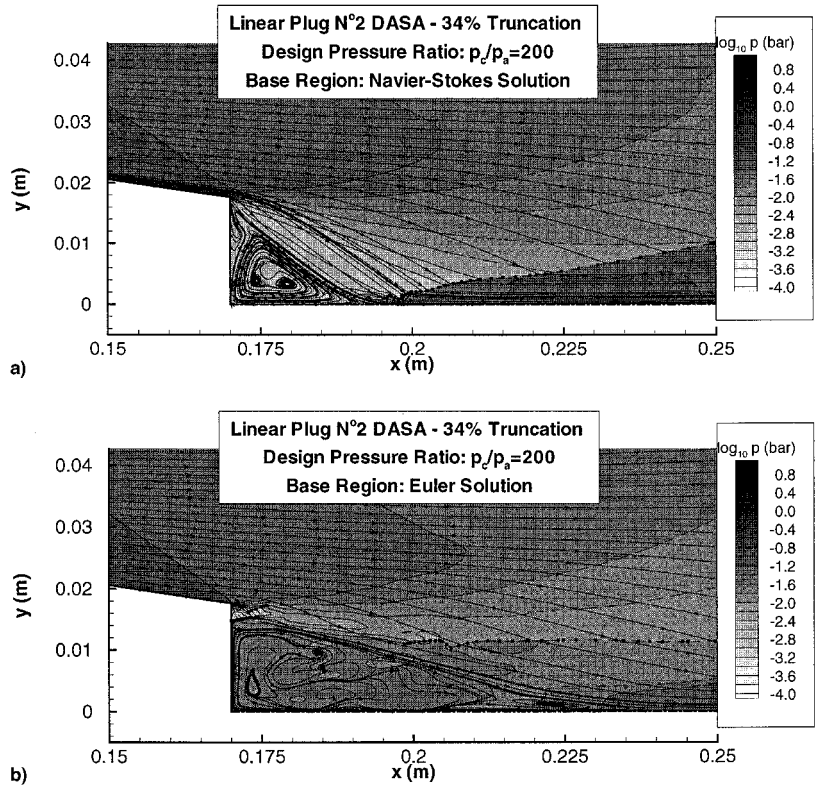

Fig. 13 Comparison of a) viscous and b) inviscid computations of the 34%-length LPN2. Pressure contours and streamlines for PR = 200.

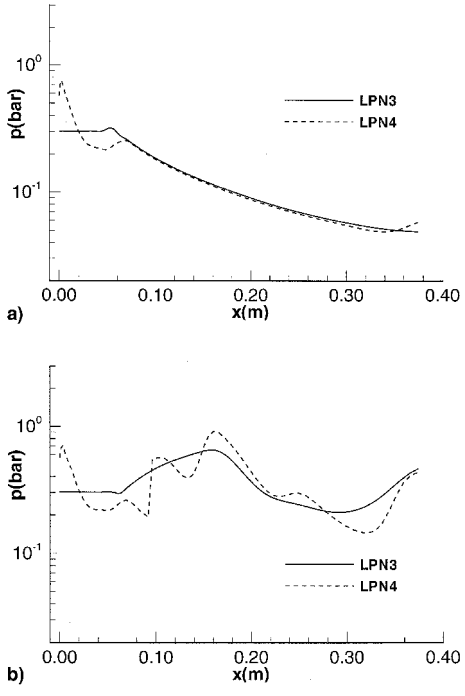

Fig. 14 Pressure along the plug wall of LPN3 (---) and LPN4 (———) for PR = a) 200 and b) 30.

mary nozzle. A comparison of the flowfield of two different full-length plug nozzles was performed for two different pressure ratios: PR = 200 and 30. The linear plug nozzles that were considered are defined as follows. The LPN3 is a plug nozzle designed by Angelino's method,[11] assuming uniform flow exhausting from the primary nozzle at the average conditions of the primary nozzle of LPN2 (exit Mach number M_e = 2.84). The LPN4 has the bell primary nozzle of LPN2, yielding nonuniform exit flow, and the same plug contour as LPN3.

Table 6 Efficiency of nozzles LPN3 and LPN4

	PR	
Nozzle	30	200
LPN3	0.99	1.00
LPN4	0.98	0.99

The results for LPN3 show a constant wall-pressure value until the first expansion wave reaches the wall. After that, the wall pressure displays a smooth behavior for both PR = 200 (Fig. 14a) and PR = 30 (Fig. 14b). This behavior is analogous to that reported in Fig. 3 for the LPN1 case, where a sonic primary nozzle (M_e = 1) exhausts uniform flow over the plug. The comparison with the more realistic case of LPN4 that features a nonuniform flow at the primary nozzle exit provides some insight on the consequences of the design assumptions.

The wall-pressure behavior for LPN4 is not as smooth as it is for LPN3, mainly because of the presence of a shock at the beginning of the plug. This shock is generated at the connection between the plug and the primary nozzle, where there is a corner because of the fact that Angelino's contour starts parallel to the primary nozzle axis (that is assumed as the average flow direction) and, therefore, at an angle with the primary nozzle divergent wall. This shock and the straight part of Angelino's contour weakens the second set of compression waves of LPN4 that is a result of the effect of the compression coming from inside the primary nozzle. Downstream, the wall-pressure behavior is equal to the ideal LPN3. In practical applications this region is therefore designed with some smooth junction between the nozzle wall exit and Angelino's plug geometry, but often it still shows problems that are usually enhanced in off-design conditions. As an example the higher-ambient-pressure case of PR = 30 is reported in this paper. The

computed behavior of wall pressure is displayed in Fig. 14b for LPN3 and LPN4. In this case there is a stronger contribution of the corner shock of LPN4. The narrower jet and the lower expansion make the shock interact sooner with the jet boundary, generating several successive reflections. An important point to emphasize is that, compared to LPN3, LPN4 yields nearly the same efficiency in both PR = 200 and 30 cases (Table 6).

Conclusions

A numerical method based on a simplified model of the jet boundary and on the fitting of flow discontinuities has shown to be a suitable tool for plug nozzle analysis. The numerical solution of full-length plug nozzle flowfields has shown their behavior as self-adaptable devices. Analyses of truncated plugs have been also performed.

The comparisons among inviscid and viscous laminar computations have shown that, for the configurations studied, the performance of plugs truncated at more than 30% of their length is comparable with full-length plugs, whereas plugs shorter than 20% have a deteriorated performance.

However, for short plugs the contribution of the base on the nozzle performance can be important, and there are still obstacles to obtaining precise predictions that are valid for all operating conditions because complex flow interaction in the base takes place and significantly changes the evaluations. In conclusion, the preceding results must be considered as first indications for the shortest plugs, and further studies are recommended to evaluate the minimum plug length so that performance will not be significantly reduced.

In particular, based on the present results, more realistic flow models including turbulence, with a detailed comparative analysis of the effects of different turbulence models, should be studied.

Acknowledgments

This study was performed through a contract with DASA in the framework of the Future European Space Transportation Investigations Programme (FESTIP) and was financed by ESA.

References

[1]Flinn, E. D., "Aerospike Engine Powers RLV Savings," *Aerospace America*, Vol. 34, No. 11, 1996, pp. 18, 19.

[2]Schoyer, H. F. R., Hufenbach, B., Morel, R., Dalbies, E., Immich, H., and Bigert, M., "Investigation of Advanced Rocket Propulsion Concepts," AIAA Paper 95-3092, July 1995.

[3]Rommel, T., Hagemann, G., Schley, C., Krulle, G., and Manski, D., "Plug Nozzle Flowfield Calculations for SSTO Applications," AIAA Paper 95-2784, July 1995.

[4]Fick, M., and Schmucker, R. H., "Remarks on Plug Cluster Nozzles," AIAA Paper 95-2694, July 1995.

[5]Nasuti, F., and Onofri, M., "Numerical Prediction of Nozzle Exhaust Plumes," *Proceedings of the 12th International Symposium on Air Breathing Engines* (Melbourne, Australia), edited by F. S. Billig, AIAA, Washington, DC, 1995, pp. 464–472.

[6]Zannetti, L., and Onofri, M., "Aerodynamics of Aircraft After Body: Numerical Simulation," AIAA Paper 84-0284, Jan. 1984.

[7]Moretti, G., "A Technique for Integrating Two-Dimensional Euler Equations," *Computer and Fluids*, Vol. 15, No. 1, 1987, pp. 59–75.

[8]Moretti, G., Marconi, F., and Onofri, M., "Shock Boundary Layer Interactions Computed by a Shock Fitting Technique," *Lecture Notes in Physics*, Vol. 414, Springer–Verlag, Berlin, 1993, pp. 345–349.

[9]Nasuti, F., and Onofri, M., "Analysis of Unsteady Supersonic Viscous Flows by a Shock Fitting Technique," *AIAA Journal*, Vol. 34, No. 7, 1996, pp. 1428–1434.

[10]Moretti, G., "Efficient Calculations of 2D Compressible Flows," *Advances in Computer Methods for PDE*, edited by R. Vichnevetsky and R. S. Stepleman, Vol. 6, IMACS, New Brunswick, NJ, 1987, pp. 60–66.

[11]Angelino, G., "Approximate Method for Plug Nozzle Design," *AIAA Journal*, Vol. 2, No. 10, 1964, pp. 1834, 1835.

[12]Broglia, R., Di Mascio, A., Favini, B., Nasuti, F., Onofri, M., and Paciorri, R., "CFD Analysis of Axisymmetric Plug Nozzle Flowfields," Technology and Research Projects, ESTEC/Contract 12019/96/NL/FG, ESA/ESTEC, Noordwijk, The Netherlands, July 1997.

[13]Tucker, P. K., "A Numerical Analysis of Supersonic Flow over an Axisymmetric Afterbody," AIAA Paper 93-2347, June 1993.

[14]Fick, M., and Schmucker, R. H., "Linear Aerospike Engine Performance Evaluation," AIAA Paper 97-3305, July 1997.